Research Square

Preprints are preliminary reports that have not undergone peer review.
They should not be considered conclusive, used to inform clinical practice,
or referenced by the media as validated information.

Graphene-Enhanced Gold Surface Plasmon Resonance Sensor for Ethanol and Methanol Refractometric Sensing

Igor Carvalho
Universidade Federal da Paraíba
Cleumar Moreira
cleumarmoreira@gmail.com
Instituto Federal do Paraná
Fabiana Fim
Universidade Federal da Paraíba

Research Article

Keywords: surface plasmon resonance; graphene; gold thin film; spectral interrogation; refractive-index sensor; ethanol; methanol

Posted Date: September 3rd, 2026

DOI: https://doi.org/10.21203/rs.3.rs-10833162/v1

License: This work is licensed under a Creative Commons Attribution 4.0 International License.
Read Full License

Additional Declarations: No competing interests reported.

Graphene-Enhanced Gold Surface Plasmon Resonance Sensor for Ethanol and Methanol Refractometric Sensing

Igor Carvalho · Cleumar Moreira · Fabiana Fim

Abstract Surface plasmon resonance (SPR) optical sensors are highly sensitive to refractive-index (RI) variations and are therefore attractive for chemical sensing. In this work, a prism-based SPR sensor comprising a gold thin film and graphene overlayers was theoretically investigated for refractometric sensing of ethanol and methanol. Gold thicknesses of 40, 50, and 65 nm were first evaluated, after which $1-20$ graphene layers were analyzed for a 50-nm Au film using a multilayer transfer-matrix model under spectral interrogation. For the selected 50-nm Au baseline, the calculated sensitivities were $2,220$, $3,242$, and $1,620$ nm/RIU for water, ethanol, and methanol, respectively. Graphene increased the maximum sensitivities to $3,540.7$ nm/RIU for water (18 layers), $4,385.3$ nm/RIU for ethanol (20 layers), and $3,190.4$ nm/RIU for methanol (20 layers), corresponding to gains of approximately 59.5%, 35.3%, and 96.9%. The best-performing graphene-coated configurations within the investigated range retained FWHM values close to 48 nm and yielded figures of merit of 73.04, 91.28, and 66.40 RIU^{-1}, respectively. Increasing graphene thickness produced a systematic redshift of the resonance wavelength and enhanced the calculated spectral response. The results indicate that graphene can improve the RI sensitivity of Au-based SPR architectures, particularly for the lower-response methanol case. Because the present analysis is based on optical modeling rather than analyte-specific recognition, experimental validation and selective surface functionalization remain necessary before chemical selectivity can be established.

Keywords surface plasmon resonance; graphene; gold thin film; spectral interrogation; refractive-index sensor; ethanol; methanol

1 Introduction

Surface plasmon resonance (SPR) is a well-established optical phenomenon widely employed in high-sensitivity chemical and biological sensing platforms [1–5]. Since its early implementation for gas detection [6], SPR has evolved into a label-free transduction technique capable of monitoring interfacial refractive-index (RI) variations in real time with high sensitivity and rapid response [7,8]. SPR sensors operate as optical refractometers: a change in the RI adjacent to the sensing surface modifies the resonance condition and shifts the measured resonance angle or wavelength.

SPR arises from the coupling of incident p-polarized light to collective oscillations of free electrons at a metal–dielectric interface [9,10]. In prism-coupled configurations, resonance occurs when the in-plane component of the incident-light wavevector matches that of the surface plasmon polariton. The resulting transfer of optical energy produces a pronounced minimum in reflected intensity whose position depends strongly on the dielectric properties of the metal and adjacent sensing medium [9,11].

Among the available excitation geometries, the Kretschmann–Raether prism configuration remains widely used because of its efficient optical coupling and straightforward implementation [12,13]. A thin plasmonic film is deposited on a high-RI prism, and total internal reflection generates the evanescent field required for plasmon excitation. Variations in the external RI can then be quantified through angular or spectral interrogation [14]. Gold is frequently selected as the plasmonic metal because of its chemical stability and resistance to oxidation [15–17]. Its resonance, however, can be broader than that obtained with silver, motivating hybrid architectures designed to improve field confinement and sensing performance [18]. Two-dimensional materials are particularly attractive as ultrathin functional overlayers. Graphene combines broadband optical response, high carrier mobility, and an atomically thin structure with a large accessible surface area [41,42,21]. Graphene-containing SPR structures have been reported to improve sensitivity in

I. Carvalho · F. Fim
Materials Science and Engineering Postgraduate Program, UFPB, 58051-900, João Pessoa, Brazil

C. Moreira (**Corresponding author**)
Informatics Department, Instituto Federal do Paraná, Colombo, PR, Brazil
E-mail: cleumar.moreira@ifpr.edu.br

several configurations [22,23], while recent studies have further demonstrated the relevance of graphene and graphene-derived interfaces for plasmonic, biochemical, and volatile-organic-compound sensing [24–26]. These developments are consistent with the broader progress of SPR sensing platforms toward hybrid material architectures [27].

Low-molecular-weight alcohols provide a useful test case because methanol and ethanol are chemically similar but have different optical properties. Methanol is toxic and its presence in beverages and fuels is a safety concern [28]; ethanol is widely used in pharmaceutical, fuel, and chemical applications, where composition and purity must be controlled [29]. Previous SPR studies have addressed alcohol sensing using prism, fiber, LSPR, and multilayer architectures [30–34]. Nevertheless, comparative spectral-interrogation studies of graphene-coated, prism-based Au sensors for ethanol and methanol remain comparatively limited.

This work therefore presents a theoretical investigation of a Kretschmann–Raether SPR sensor based on Au with 1–20 graphene layers. Spectral reflectance, resonance wavelength, sensitivity, FWHM, and figure of merit (FOM) are evaluated. The purpose is to quantify how graphene thickness modifies the optical response and to identify configurations that improve RI sensitivity while retaining a sufficiently narrow resonance. The analysis is explicitly refractometric: analyte-specific adsorption and chemical selectivity are not included in the transfer-matrix model and must be addressed in future experimental studies.

2 Methodology

2.1 Optical model and sensor structure

Figure 1 illustrates the prism-coupled SPR configuration. A p-polarized beam is incident through the prism onto the metal film. Under total internal reflection, the evanescent field couples to a surface plasmon when the phase-matching condition is satisfied. The reflected spectrum is then used to identify the resonance wavelength.

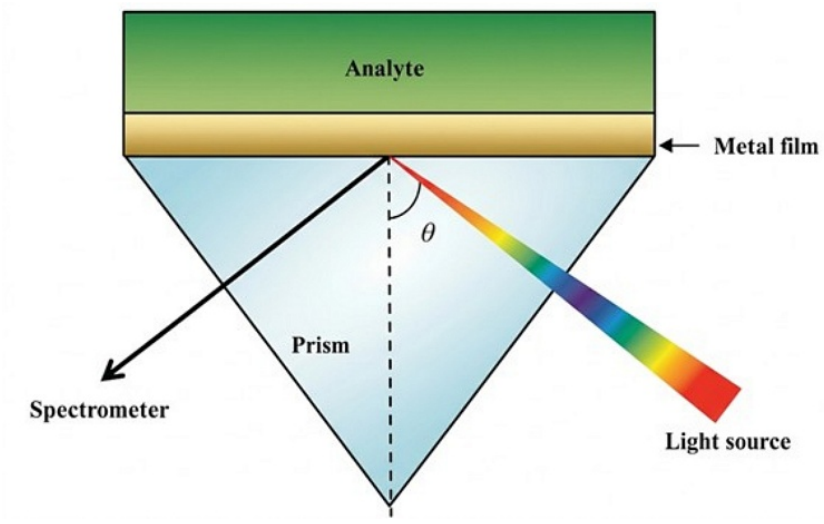


Fig. 1 Schematic diagram of the prism-based SPR sensor configuration.

The in-plane propagation constant of the optical evanescent wave is written as [35]

$$K_{\mathrm{OE}} = \frac{\omega}{c}\sqrt{\varepsilon_c}\sin\theta, \tag{1}$$

where ε_c is the dielectric constant of the prism, θ is the incidence angle, ω is the angular frequency, and c is the speed of light in vacuum. The surface-plasmon wavevector at a metal/sensing-medium interface is

$$K_{\mathrm{SP}} = \frac{\omega}{c}\left(\frac{\varepsilon_m\varepsilon_s}{\varepsilon_m+\varepsilon_s}\right)^{1/2}, \tag{2}$$

where ε_m and ε_s denote the dielectric functions of the metal and sensing medium, respectively. SPR occurs when $K_{\mathrm{OE}} = K_{\mathrm{SP}}$.

The coupling prism was made of BK7 glass. The spectral simulations were performed at a fixed incidence angle of 72.54° using 10,000 wavelength points distributed over the range from 400 to 1,000 nm. The wavelength-dependent refractive-index data used for the material layers were obtained by cubic-spline interpolation of the optical data reported by McPeak et al. and made available through the RefractiveIndex.INFO database [19,20]. The database was accessed on January 7, 2019. No temperature was specified for the analyte refractive indices in the original simulation.

2.2 Transfer-matrix method

The multilayer system is modeled using the transfer-matrix method, with each layer assumed homogeneous, isotropic, and non-magnetic. Complex refractive indices, $\tilde{n} = n + i\kappa$, account for propagation and absorption in the metallic and graphene layers. For layer k, the characteristic matrix can be written as [35]

$$M_k = \begin{bmatrix} \cos\beta_k & -i\,\sin\beta_k/q_k \\ -i\,q_k\sin\beta_k & \cos\beta_k \end{bmatrix}, \tag{3}$$

where β_k is the phase thickness and q_k is the optical admittance for p polarization. After multiplication of the individual layer matrices, the p-polarized reflection coefficient is

$$r_p = \frac{(m_{11} + m_{12}q_N)q_1 - (m_{21} + m_{22}q_N)}{(m_{11} + m_{12}q_N)q_1 + (m_{21} + m_{22}q_N)}, \tag{4}$$

and the reflectance is

$$R_p = |r_p|^2. \tag{5}$$

The resonance wavelength λ_{res} is defined as the wavelength corresponding to the minimum of R_p. The FWHM was extracted directly from the simulated reflectivity values for each resonance curve.

2.3 Performance parameters

For spectral interrogation, RI sensitivity is defined as [36]

$$S_n = \frac{\Delta\lambda_{\mathrm{res}}}{\Delta n_{\mathrm{ext}}} \quad [\mathrm{nm/RIU}], \tag{6}$$

where Δn_{ext} is the change in external RI. The FOM is defined as [37,38]

$$\mathrm{FOM} = \frac{S_n}{\mathrm{FWHM}} \quad [\mathrm{RIU}^{-1}]. \tag{7}$$

Thus, higher FOM values correspond to a favorable combination of large spectral sensitivity and narrow resonance bandwidth.

2.4 Graphene optical model

Each graphene layer is modeled with a thickness of approximately 0.34 nm. Following the optical-constant model used in the original study [41,42], the complex refractive index is represented as

$$\tilde{n}_g = 3.0 + i\frac{C\lambda}{3}, \tag{8}$$

where $C = 5.446\ \mu\mathrm{m}^{-1}$ and λ must be expressed in units consistent with C. This empirical representation is used to examine the effect of increasing graphene thickness from 1 to 20 layers.

3 Results and Discussion

3.1 Conventional gold SPR sensor

Figure 2 shows the simulated spectral reflectance for water, ethanol, and methanol as the Au thickness is varied. The 50-nm Au film produces the deepest and most clearly defined resonance among the configurations emphasized in the original analysis and is therefore adopted as the common baseline for the graphene study. Importantly, this choice is based on resonance quality and a cross-analyte compromise rather than on maximizing every individual metric: Table 1 shows that the highest sensitivity or FOM for a given analyte can occur at 40 or 65 nm.

For the selected 50-nm film, the sensitivity is $2,220$ nm/RIU for water. The corresponding values are $3,242$ nm/RIU for ethanol and $1,620$ nm/RIU for methanol. The FWHM values are approximately 49.7 nm. Ethanol therefore gives the largest calculated spectral sensitivity among the three media, whereas methanol gives the smallest. Within the present optical model, these differences should primarily be interpreted in terms of the dielectric properties assigned to the sensing media and their effect on the SPR dispersion relation; analyte-specific adsorption is not explicitly modeled.

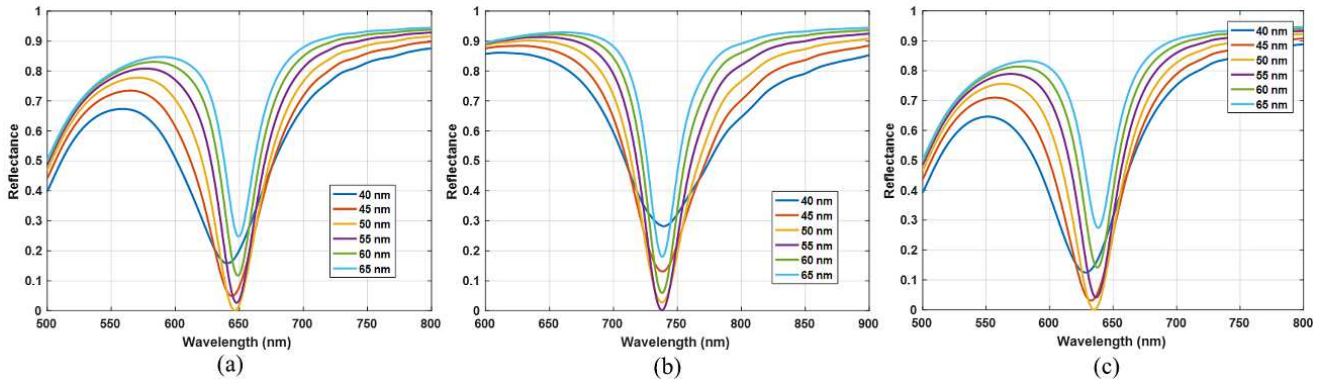


Fig. 2 Simulated reflectance curves of the prism-based Au SPR sensor for (a) distilled water, (b) ethanol, and (c) methanol for the investigated Au thicknesses.

Table 1 Performance parameters of conventional Au-based SPR sensors for water, ethanol, and methanol.

Analyte	Au thickness (nm)	Sensitivity (nm/RIU)	FWHM (nm)	FOM (RIU^{-1})
Water	40	2, 180	85.95	25.36
Water	50	2, 220	49.70	44.66
Water	65	2, 005	32.30	62.07
Ethanol	40	3, 504	94.90	36.92
Ethanol	50	3, 242	49.71	65.25
Ethanol	65	3, 146	32.16	97.83
Methanol	40	1, 740	85.96	20.22
Methanol	50	1, 620	49.70	32.59
Methanol	65	1, 569	32.16	48.81

3.2 Graphene-coated gold SPR sensor

Figures 3–5 show the response obtained after adding $1-20$ graphene layers to the 50-nm Au film. Increasing graphene thickness shifts the resonance toward longer wavelengths and modifies the sensitivity. Because the simulated observation window extends to $1,000$ nm, configurations whose resonance approaches or exceeds this upper limit should be interpreted cautiously when considering practical spectral interrogation.

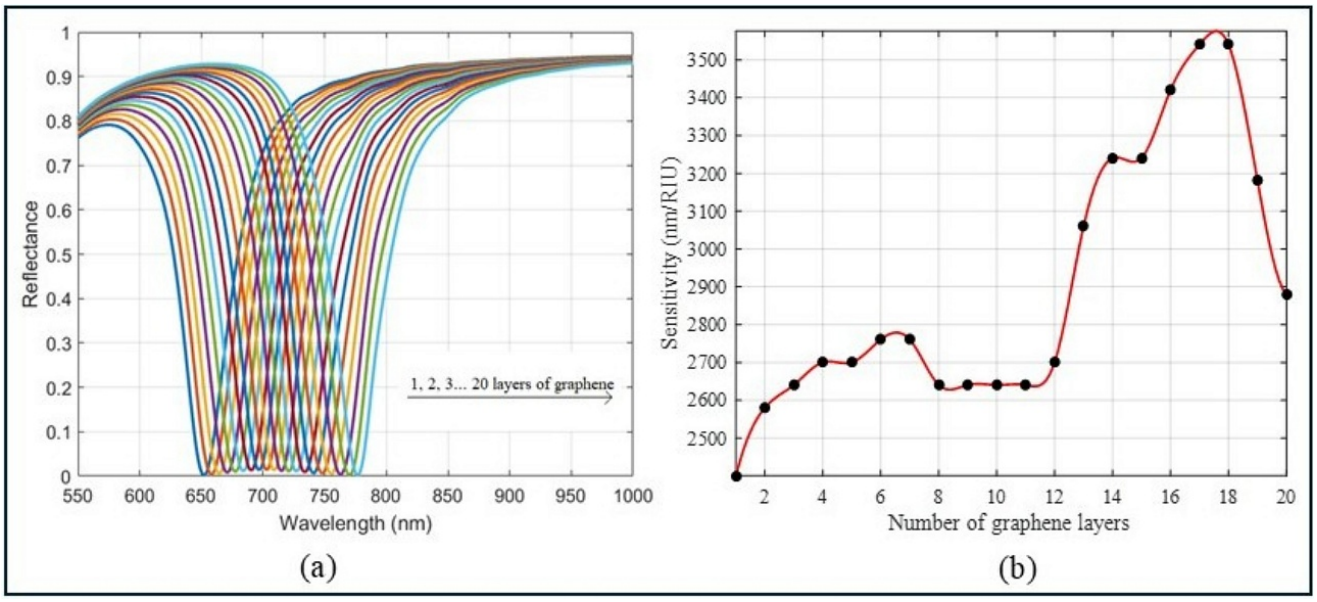


Fig. 3 (a) Reflectance curves of the 50-nm Au SPR sensor with $1-20$ graphene layers for distilled water and (b) corresponding sensitivity values.

For water, the response reaches a maximum region around $17-18$ graphene layers. The 18-layer configuration gives $S_n = 3,540.7$ nm/RIU, FWHM = 48.47 nm, and FOM = 73.04 RIU^{-1}. Relative to the 50-nm bare-Au baseline, the sensitivity gain is approximately 59.5%.

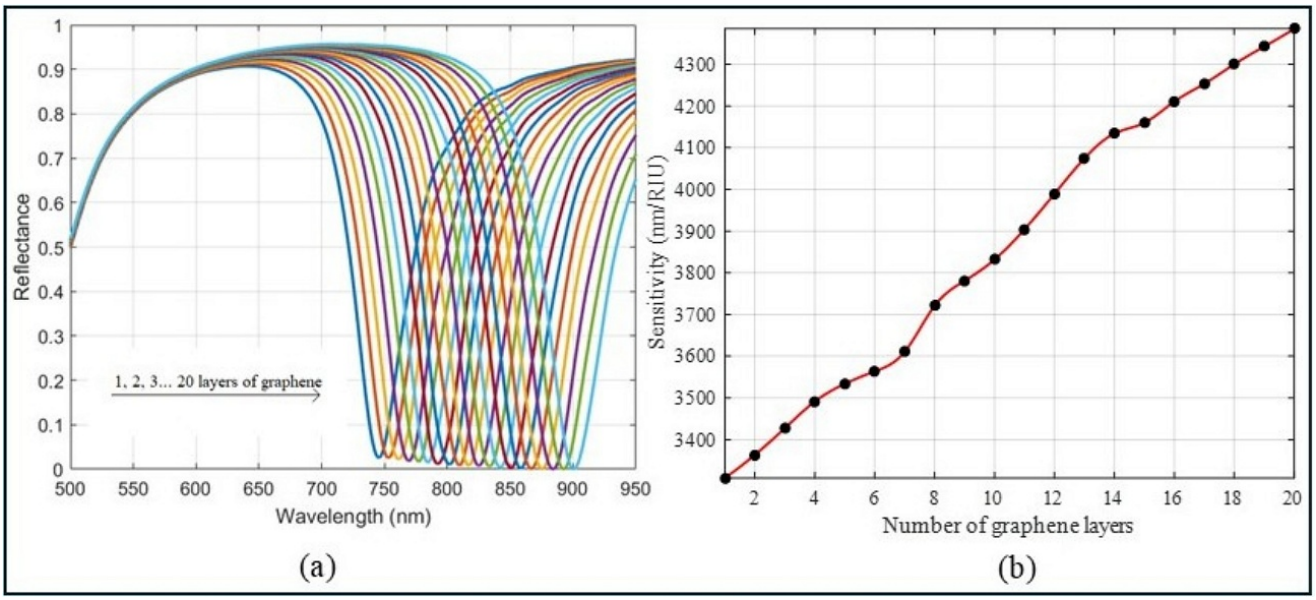


Fig. 4 (a) Reflectance curves of the 50-nm Au SPR sensor with $1-20$ graphene layers for ethanol and (b) corresponding sensitivity values.

For ethanol, sensitivity increases over the modeled graphene-layer range and reaches $4,385.3$ nm/RIU at 20 layers, with FWHM = 48.04 nm and FOM = 91.28 RIU^{-1}. This corresponds to a 35.3% sensitivity increase relative to the 50-nm bare-Au configuration. The resonance also moves progressively toward the upper limit of the modeled spectral window, which may constrain the usable layer number in an experimental instrument with a $1,000$-nm upper detection limit.

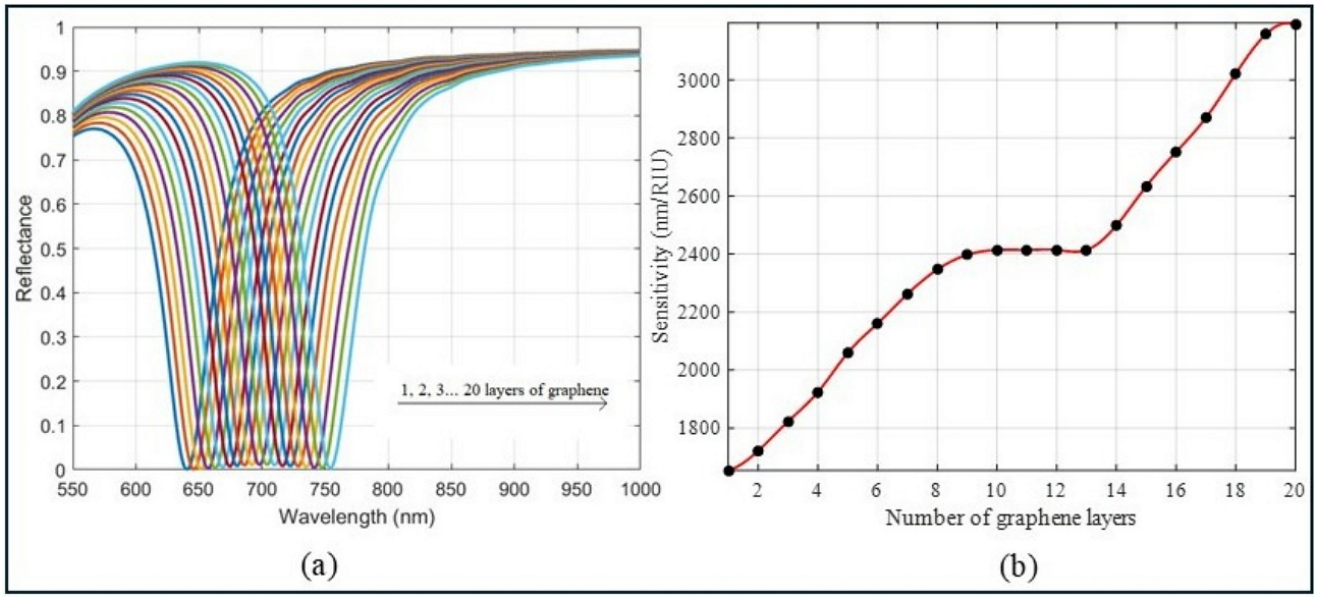


Fig. 5 (a) Reflectance curves of the 50-nm Au SPR sensor with $1-20$ graphene layers for methanol and (b) corresponding sensitivity values.

For methanol, the 20-layer configuration gives $S_n = 3,190.4$ nm/RIU, FWHM = 48.02 nm, and FOM = 66.40 RIU^{-1}. Relative to the 50-nm bare-Au baseline ($1,620$ nm/RIU), this is a calculated sensitivity increase of approximately 96.9%, making methanol the case with the largest relative improvement.

Table 2 Selected graphene-coated configurations and their calculated performance. Percentage gains are recalculated relative to the 50-nm bare-Au baseline in Table 1.

Analyte	Graphene layers	Sensitivity (nm/RIU)	FWHM (nm)	FOM (RIU^{-1})
Water	18	3,540.7 (+59.5%)	48.47	73.04
Ethanol	20	4,385.3 (+35.3%)	48.04	91.28
Methanol	20	3,190.4 (+96.9%)	48.02	66.40

The nearly constant FWHM values of the selected graphene-coated cases indicate that the modeled sensitivity enhancement is not accompanied by substantial broadening at these operating points. This is reflected in the corresponding FOM values. The layer-dependent response is not strictly monotonic for all sensing media because increasing graphene thickness modifies the effective optical admittance and electromagnetic-field distribution of the multilayer stack, thereby changing the wavelength-dependent phase-matching condition. Consequently, the local displacement of the resonance with external RI can vary with both graphene thickness and the dielectric properties of the sensing medium. Nevertheless, the number of graphene layers should not be interpreted as universally optimal: the useful thickness depends on analyte RI, spectral range, material losses, and the practical ability to fabricate uniform multilayer graphene coatings. Accordingly, the configurations reported in Table 2 are best-performing cases within the investigated range rather than universally optimal structures.

Previous atomistic studies indicate that alcohol molecules can interact differently with pristine or defective graphene surfaces [43,44]. Such results may be relevant to future functionalized devices, but they are not part of the present transfer-matrix calculation. Consequently, the sensitivity differences obtained here should not be attributed directly to binding energy or adsorption affinity. Establishing chemical selectivity between ethanol and methanol would require an analyte-specific interfacial model and, ultimately, experimental validation.

3.3 Comparison with related graphene-based SPR sensors

Table 3 compares the calculated ethanol sensitivity with representative graphene-containing SPR architectures reported in the literature. Direct comparison should be made cautiously because geometry, interrogation method, wavelength range, material model, and experimental/theoretical conditions differ among studies.

Table 3 Representative spectral sensitivities reported for graphene-containing SPR sensors evaluated with aqueous ethanol or ethanol solutions. Differences in architecture and experimental or theoretical conditions limit direct comparison.

Configuration	Analyte	Sensitivity (nm/RIU)	Reference
G/HMM/D-POF SPR sensor	Aqueous ethanol	5,166.7	[45]
D-shaped fiber, graphene/Au/MIP	Ethanol	1,137	[31]
D-POF/Au/graphene	Ethanol solution	1,223	[46]
FBG/Au/graphene oxide	Aqueous ethanol	500	[47]
PMMA prism/Au/graphene	Ethanol	4,385	This work

The present prism-based model yields a competitive spectral sensitivity for ethanol while retaining a comparatively simple Au/graphene stack. A reported prism-based methanol sensor [48] was not included in Table 3 because it uses angular interrogation, making a direct numerical comparison with spectral sensitivity in nm/RIU inappropriate without a common conversion framework.

4 Conclusions

A theoretical spectral-interrogation analysis of a prism-based Au/graphene SPR sensor was performed for water, ethanol, and methanol. A 50-nm Au film was selected as a common baseline because it provided a pronounced resonance and a practical cross-analyte compromise, although other Au thicknesses maximize individual metrics. Adding graphene produced a systematic resonance redshift and increased the calculated RI sensitivity. The selected configurations reached 3,540.7 nm/RIU for water with 18 graphene layers, 4,385.3 nm/RIU for ethanol with 20 layers, and 3,190.4 nm/RIU for methanol with 20 layers, corresponding to sensitivity gains of approximately 59.5%, 35.3%, and 96.9% relative to the 50-nm bare-Au baseline. The associated FWHM values remained close to 48 nm, giving FOM values of 73.04, 91.28, and 66.40 RIU^{-1}, respectively.

These results support graphene as a promising optical enhancement layer for Au-based SPR refractometric sensing. However, the present model does not establish molecular selectivity between ethanol and methanol because it does not explicitly include adsorption kinetics, binding specificity, cross-interference, or experimental uncertainty. Future work

should therefore validate the predicted trends experimentally, report complete optical and numerical parameters, assess fabrication tolerances, and investigate selective functionalization when chemical identification rather than RI sensing is required.

Acknowledgements

I. Carvalho and F. Fim gratefully acknowledge PROPESQ/PRPG/UFPB (PIF13399-2020) for partial financial support. C. Moreira acknowledges the support provided by the Virtus Research, Development, and Innovation Center, including VIRTUS-CC (EMBRAPII VIRTUS Competence Center – Intelligent Hardware for Industry), at the Federal University of Campina Grande. This initiative is supported by EMBRAPII (Brazilian Company for Industrial Research and Innovation) through funding from the Brazilian Ministry of Science, Technology and Innovation (MCTI) under the PPI HardwareBR program.

Declarations

Ethics approval. Not applicable.
Competing interests. The authors declare no competing interests.
Funding. Partial financial support was provided by PROPESQ/PRPG/UFPB (PIF13399-2020). Support associated with VIRTUS-CC was provided through EMBRAPII funding from MCTI under the PPI HardwareBR program.
Data availability. The numerical results supporting the findings of this theoretical study are presented within the article. Additional simulation data may be made available by the corresponding author upon reasonable request.
Author contributions. I. Carvalho: investigation, numerical simulations, data analysis, and figure preparation. F. Fim: supervision, interpretation of results, writing–review and editing. C. Moreira: conceptualization, methodology, supervision, interpretation of results, writing–review and editing. All authors reviewed and approved the final manuscript.

References

1. B. B. Motsa and R. V. Stahelin, "A beginner's guide to surface plasmon resonance," Biochem. (Lond). 45(1), 18–22 (2023). doi:10.1042/bio_2022_139.
2. Y. Terada et al., "SPR study for analysis of a water-soluble glycopolymer interface and molecular recognition properties," Polym. J. 49(2), 255–262 (2017). doi:10.1038/pj.2016.99.
3. C. M. Miyazaki, F. M. Shimizu, and M. Ferreira, "Surface Plasmon Resonance (SPR) for Sensors and Biosensors," in Nanocharacterization Techniques, Elsevier, pp. 183–200 (2017). doi:10.1016/B978-0-323-49778-7.00006-0.
4. X. Wang, M. Ma, X. Wang, and S. Wang, "Surface Plasmon Resonance Sensors for Concentration and Reaction Kinetic Detections," in Analytical Chemistry–Advancement, Perspectives and Applications, IntechOpen (2021). doi:10.5772/intechopen.92549.
5. M. A. Butt, "Surface Plasmon Resonance-Based Biodetection Systems: Principles, Progress and Applications—A Comprehensive Review," Biosensors 15(1), 35 (2025). doi:10.3390/bios15010035.
6. V. Kumar, S. K. Raghuwanshi, and S. Kumar, "Realization of prism-based surface plasmon resonance sensor for detection of methane gas," Proc. SPIE (2023). doi:10.1117/12.2648959.
7. A. S. Kushwaha et al., "A study of surface plasmon resonance (SPR) based biosensor with improved sensitivity," Photonics Nanostruct. 31, 99–106 (2018). doi:10.1016/j.photonics.2018.06.003.
8. Y. Zeng et al., "Recent advances in surface plasmon resonance imaging: detection speed, sensitivity, and portability," Nanophotonics 6(5), 1017–1030 (2017). doi:10.1515/nanoph-2017-0022.
9. V. N. Kannan, G. Prabhakar, and N. Ayyanar, "Surface plasmon resonance sensor with 2D materials for enhanced refractive index detection of chemical pollutants in seawater," Optik 321, 172157 (2025). doi:10.1016/j.ijleo.2024.172157.
10. S. Kumar, G. Sharma, and V. Singh, "Modelling of surface plasmon resonance sensor for detection of mass concentration of ethanol and methanol in a binary mixture," Infrared Phys. Technol. 67, 190–196 (2014). doi:10.1016/j.infrared.2014.07.021.
11. G. A. Khan, Y. Lu, and P. Wang, "Plasmon-Enhanced Refractive Index Sensing of Biomolecules Based on Metal–Dielectric–Metal Metasurface in the Infrared Regime," ACS Omega 9(1), 1416–1423 (2024). doi:10.1021/acsomega.3c07809.
12. P. S. Pandey, S. K. Raghuwanshi, and S. Kumar, "Recent Advances in Two-Dimensional Materials-Based Kretschmann Configuration for SPR Sensors: A Review," IEEE Sens. J. 22(2), 1069–1080 (2022). doi:10.1109/JSEN.2021.3133007.
13. N. Shukla et al., "Surface Plasmon Resonance Biosensors Based on Kretschmann Configuration: Basic Instrumentation and Applications," pp. 191–222 (2022). doi:10.1007/978-3-030-99491-4_6.
14. M. Kanso, S. Cuenot, and G. Louarn, "Sensitivity of Optical Fiber Sensor Based on Surface Plasmon Resonance: Modeling and Experiments," Plasmonics 3, 49–57 (2008). doi:10.1007/s11468-008-9055-1.
15. W. Fang et al., "Prism SPR Glucose Sensor Based on Gold Nanoparticle/Gold Film Coupling Enhanced SPR," IEEE Sens. J. 23(12), 12477–12484 (2023). doi:10.1109/JSEN.2023.3268310.
16. N. F. Murat et al., "Optimization of gold thin films thicknesses in enhancing SPR response," Proc. ICSE, 244–247 (2016). doi:10.1109/SMELEC.2016.7573637.
17. H. Suzuki et al., "Effects of gold film thickness on spectrum profile and sensitivity of a multimode-optical-fiber SPR sensor," Sens. Actuators B Chem. 132(1), 26–33 (2008). doi:10.1016/j.snb.2008.01.003.
18. Y. Li et al., "Silver-Based Surface Plasmon Sensors: Fabrication and Applications," Int. J. Mol. Sci. 24(4), 4142 (2023). doi:10.3390/ijms24044142.
19. K. M. McPeak et al., "Plasmonic Films Can Easily Be Better: Rules and Recipes," ACS Photonics 2(3), 326–333 (2015). doi:10.1021/ph5004237.
20. M. N. Polyanskiy, "Refractive index database," `https://refractiveindex.info` (accessed January 7, 2019).

21. Y. Singh et al., "Sensitivity Enhancement of SPR Sensor with the Black Phosphorus and Graphene with Bi-layer of Gold for Chemical Sensing," Plasmonics 16(5), 1781–1790 (2021). doi:10.1007/s11468-020-01315-3.
22. Z. Zhao and Q. Wang, "Gold nanoparticles and graphene oxide heterostructures with gold film coupling for an enhanced sensitivity SPR fiber sensor," Instrum. Sci. Technol. 50(5), 530–542 (2022). doi:10.1080/10739149.2022.2044845.
23. I. Carvalho et al., "A Field-Enhancement Optical Fiber SPR Sensor Using Graphene, Molybdenum Disulfide, and Zinc Oxide," Plasmonics 18(5), 1705–1713 (2023). doi:10.1007/s11468-023-01880-3.
24. K. Drozdowska et al., "Plasmon-Induced Graphene/Silicon Schottky Junctions for Ultrasensitive Gas Sensing," ACS Sens. 10(10), 7650–7660 (2025). doi:10.1021/acssensors.5c01920.
25. Y. Singh et al., "Highly Sensitive Graphene-Assisted Large-Area Kapton-Based Flexible Surface Plasmon Resonance Biosensor for Enzymatic Glucose Detection," ACS Appl. Mater. Interfaces 17(32), 45527–45537 (2025). doi:10.1021/acsami.5c09827.
26. H. Selvi et al., "Sensing volatile organic compounds with CVD graphene: insights from quartz crystal microbalance and surface plasmon resonance studies," J. Mater. Sci.: Mater. Electron. 35(18), 1268 (2024). doi:10.1007/s10854-024-13087-1.
27. V. Yesudasu, H. S. Pradhan, and R. J. Pandya, "Recent progress in surface plasmon resonance based sensors: A comprehensive review," Heliyon 7(3), e06321 (2021). doi:10.1016/j.heliyon.2021.e06321.
28. M. Abubakar et al., "Methanol Formation, Toxicity and its Impact on the Human Nervous System and Liver," Pakistan Journal of Health Sciences, 12–20 (2023). doi:10.54393/pjhs.v4i10.1056.
29. S. Paprocki, M. Qassem, and P. A. Kyriacou, "Review of Ethanol Intoxication Sensing Technologies and Techniques," Sensors 22(18), 6819 (2022). doi:10.3390/s22186819.
30. V. Kumar et al., "Nanocomposite Thin Film-Based Surface Plasmon Sensor for Detection of Ethanol in Petrochemical Industries," IEEE Trans. Plasma Sci. 52(2), 328–335 (2024). doi:10.1109/TPS.2023.3337175.
31. V. Sharma et al., "Graphene/Au/MIP-Coated D-Shaped Optical Fiber–Based SPR Sensor for Ethanol Detection," Plasmonics 18(5), 1639–1649 (2023). doi:10.1007/s11468-023-01920-y.
32. S. Liu et al., "Optical fiber SPR ethanol gas sensor based on perovskite," Proc. CCDC, 1192–1195 (2022). doi:10.1109/CCDC55256.2022.10033564.
33. S. Dixit, P. Kumar, and R. K. Verma, "Localized Surface Plasmon Resonance Based Fiber Optic Ethanol and Methanol Sensor Using UV light based AgNO_3/ZnO Nanorods," 13th International Conference on Fiber Optics and Photonics, Th3A.58 (2016). doi:10.1364/PHOTONICS.2016.Th3A.58.
34. M. E. Ouardi et al., "Detection of Water-alcohol Content Using Surface Plasmon Resonance," Plasmonics 20(1), 399–406 (2024). doi:10.1007/s11468-024-02285-6.
35. L. Wu et al., "Highly sensitive graphene biosensors based on surface plasmon resonance," Opt. Express 18(14), 14395 (2010). doi:10.1364/OE.18.014395.
36. Y. Yuan, L. Ding, and Z. Guo, "Numerical investigation for SPR-based optical fiber sensor," Sens. Actuators B Chem. 157(1), 240–245 (2011). doi:10.1016/j.snb.2011.03.056.
37. Y. S. Dwivedi, A. K. Sharma, and B. D. Gupta, "Influence of Design Parameters on the Performance of a Surface Plasmon Sensor Based Fiber Optic Sensor," Plasmonics 3, 79–86 (2008). doi:10.1007/s11468-008-9057-z.
38. J.-T. Lin et al., "Analysis of Scaling Law and Figure of Merit of Fiber-Based Biosensor," J. Nanomater. 2012 (2012). doi:10.1155/2012/154736.
39. H. Song, Q. Wang, and W.-M. Zhao, "A novel SPR sensor sensitivity-enhancing method for immunoassay by inserting MoS_2 nanosheets between metal film and fiber," Opt. Lasers Eng. 132, 106135 (2020). doi:10.1016/j.optlaseng.2020.106135.
40. W. Wei et al., "Graphene/Au-Enhanced Plastic Clad Silica Fiber Optic Surface Plasmon Resonance Sensor," Plasmonics 13(2), 483–491 (2018). doi:10.1007/s11468-017-0534-0.
41. M. Bruna and S. Borini, "Optical constants of graphene layers in the visible range," Appl. Phys. Lett. 94(3) (2009). doi:10.1063/1.3073717.
42. R. R. Nair et al., "Fine Structure Constant Defines Visual Transparency of Graphene," Science 320(5881), 1308 (2008). doi:10.1126/science.1156965.
43. V. B. T. Phung et al., "Graphene as a Sensor for Lung Cancer: Insights into Adsorption of VOCs Using vdW DFT," ACS Omega 9(2), 2302–2313 (2024). doi:10.1021/acsomega.3c06159.
44. S. Dandeliya and A. Srivastava, "Electron transport in ethanol & methanol absorbed defected graphene," AIP Conf. Proc., 140140 (2018). doi:10.1063/1.5033315.
45. J. Gao et al., "Enhanced sensitivity of a surface plasmon resonance biosensor using hyperbolic metamaterial and monolayer graphene," Opt. Express 29(26), 43766 (2021). doi:10.1364/OE.447107.
46. X. Xi et al., "An Au Nanofilm-Graphene/D-Type Fiber Surface Plasmon Resonance Sensor for Highly Sensitive Specificity Bioanalysis," Sensors 20(4), 991 (2020). doi:10.3390/s20040991.
47. P. T. Arasu et al., "Fiber Bragg grating assisted surface plasmon resonance sensor with graphene oxide sensing layer," Opt. Commun. 380, 260–266 (2016). doi:10.1016/j.optcom.2016.05.081.
48. A. K. Sharma and A. Dominic, "Coordinated Tuning of Graphene's Chemical Potential with NIR Wavelength and Temperature under Kubo Framework for Enhanced Performance of SPR-Based Chemical Sensor," IEEE Sens. J. 18(22), 9207–9213 (2018). doi:10.1109/JSEN.2018.2870743.